Asymmetric Tug-of-War leads to Cooperative Transport of a Cargo by Multiple Kinesins

Marco Tjioe[1,2,3,*], Saurabh Shukla[2,4], Rohit Vaidya[1,2], Alice Troitskaia[1], Carol Bookwalter[5], Kathleen M. Trybus[5], Yann R. Chemla[1,2,3], Paul R. Selvin[1,2,3,**]

[1]Center for Biophysics and Quantitative Biology, [2]Center for the Physics of Living Cells, [3]Department of Physics, [4]Department of Chemical and Biomolecular Engineering, University of Illinois at Urbana-Champaign, Urbana, Illinois 61801, United States
[5]Department of Molecular Physiology and Biophysics, University of Vermont, Burlington, VT 05405
*Current address: Indiana Biosciences Research Institute, Indianapolis, IN 46202.
**Corresponding author: selvin@illinois.edu

Abstract

How cargoes move within a crowded cell—over long distances and at speeds that are nearly the same as when moving on an unimpeded pathway—has long been mysterious. Through an *in vitro* gliding assay, which involves measuring nanometer displacement and piconewtons of force, we have evidence that when kinesins, a cytoplasmic molecular motor, operate in small groups, from 2-10, they can communicate among themselves through an asymmetric tug-of-war by inducing tension (up to 4 pN) on the cargo. Surprisingly, the primary role of approximately one-third of kinesins is to develop tension, which instantaneously slows forward motion but helps increase cargo run length. These hindering kinesins fall off rapidly when experiencing a forward tug. Occasionally, they may be ripped off from their anchors by other driving kinesins working in tandem. Furthermore, with roadblocks on the microtubule, multiple kinesins cooperate to overcome impediments. Hence, kinesin may employ an asymmetric tug-of-war *and* a cooperative motion to navigate through cellular environment.

Main Text

Kinesin is a cytoskeletal motor that moves cellular cargoes primarily towards the plus end of microtubules or the cell periphery. Kinesin, similar to other motors such as dynein and myosin, is important in key cellular processes such as organelle transport, cell division, and cell signaling[1], and has been implicated in several neurological diseases including Alzheimer's and Parkinson's.[2] Due to advances in single molecule microscopy and force measurement techniques, transport properties of a single kinesin are understood in great detail[3]. For example, kinesin-1, the prototypical kinesin, moves 8.4 nm per ATP consumed, in a hand-over-hand motion, walking about 100 steps before detaching and traveling at a speed of 0.77 μm/sec *in vitro*[6] and equal or higher speed *in vivo*[4–7]. A single kinesin also exerts up to ~6 pN force[8], and importantly, has an asymmetric response to force in terms of run length and velocity (Fig. 1a,b).[9,10]

How do cargoes move in the cell, which is highly dense and filled with numerous roadblocks and detours, at approximately the same speed as it moves through an unimpeded pathway typically found *in vitro*? The answer is unclear, although it was found that multiple motors, ranging from 2-10, including teams of similar and dissimilar motors, help cargoes transport through "traffic jams" and increase the path-length that the cargo is carried.[11–14] How do multiple motors avoid impeding one another, especially when one is stuck? One intriguing possibility is the presence of an asymmetric release mechanism. Impeding kinesins will tend to detach rapidly, leaving the forward-driving kinesin to continue on. Such an asymmetric response to force may also help maintain uninterrupted transport. Yet, none of these cooperative behavior have been shown to

work on cargoes with multiple motors. Even the cooperative nature of kinesin is unclear, with opposite conclusions presented in a recent review.[15]

To examine this issue, we have investigated multiple kinesins pulling simultaneously on a single cargo via a gliding assay that is also capable of measuring the force pulled by the kinesin. We call this a force-gliding assay (Fig. 1c).[16] A gliding assay is essentially an inverted walking-type assay, where the microtubule is the cargo[17]. Fortunately, the two methods yield virtually identical results: $v_{gliding}$ = 931 ± 77 nm/sec for a single kinesin driving a microtubule (n=6291; Fig. 3f for single kinesin); $v_{walking}$ = 1148 ± 281 nm/sec for a single kinesin walking on a microtubule (n=786) (Supplementary Fig. S2), although it is very temperature sensitive[18].

In the force-gliding assay, each kinesin was labeled with a quantum dot and attached by a 1565-base dsDNA, which acts like a nonlinear spring, to a non-stick polyethylene-glycol (PEG) coverslip. A fluorescently-labeled microtubule (shown moving to the right in Fig. 1c) served as the cargo and was moved by kinesin (moving to the left) at 1 mM ATP. The kinesin either speeds up the microtubule as evidenced by the kinesin staying to the left of the equilibrium position, called the "driving kinesin", or slowing the microtubule down, in which case it resides to the right and is called the "hindering kinesin". Each kinesins' position can be individually monitored with nanometer displacement via a tracking algorithm similar to Fluorescence Imaging with One Nanometer Accuracy (FIONA)[19] (see Methods). Single particle tracking was possible because the kinesins were placed greater than a diffraction-limited distance apart and hence each individual kinesin can be monitored simutaneously. The DNA acts like an extensible Worm Like Chain (eWLC), where the magnitude of the force on the microtubule by each kinesin is non-linearly proportional to the DNA extension[20]. Both signals from the QD on the kinesin and the fluorophores on the microtubule allow minutes-long recording.

Fig. 1d,e is an example of a microtubule (green) transported by three kinesins, labeled # 1,2,3. Fig. 1d shows the microscope raw images and Fig. 1e the microtubule kymograph, velocity and kinesin displacements. Yellow arrows in Fig. 1d show the equilibrium positions of the kinesins when no force is exerted on the microtubule (i.e. when kinesin is not attached to microtubule); white arrows show forces from kinesins on microtubule as the kinesins are displaced from equilibrium, and the red arrows show the direction of microtubule movement. Four time points (0, 1.5, 5.2 and 14.0 seconds) are shown in Fig. 1d, taken every 0.2 sec. These time points are marked with orange vertical lines in Fig. 1e. Regions marked 1', 2' and 3' in Fig. 1e corresponds to typical driving/ hindering behavior, starting with a transition away from equilibrium (1'), constant displacement from equilibrium (2') and return to equilibrium (3'). At time 0 kinesins are at their equilibrium positions. At 1.5 sec, a microtubule becomes present. Kinesin #1 and #3 are still at the equilibrium positions; while kinesin #2 rapidly starts driving the microtubule. Its absolute position (with regard to the coverslip) in Fig. 1d shows that kinesin #2 has moved leftwards (downward displacement in Fig. 1e), causing it to be rapidly displaced by ~ -350 nm. It then remains at -350 nm from equilibrium; meaning its absolute velocity (relative to the coverslip) is zero. At this point, the net force on the kinesin is zero: the backward force on the kinesin due to the ATP-driven microtubule is counterbalanced by the forward force on the kinesin by the DNA linker. The microtubule velocity, as visualized by the kymograph and a display of its velocity (Fig. 1e) then suddenly increased from zero to ~850 nm/sec, evidently the fastest the microtubule can go in this trace. At 5.2 sec, kinesin #2 is still driving the microtubule but with apparently less force—inferred from the displacement (using eWLC, discussed below), as shown in Fig. 1e. Kinesin #1 is now also driving the microtubule and kinesin #3 is hindering the microtubule. The net result is that the microtubule is still going at ~850 nm/sec. At 14.0 sec, kinesin #1 has reached

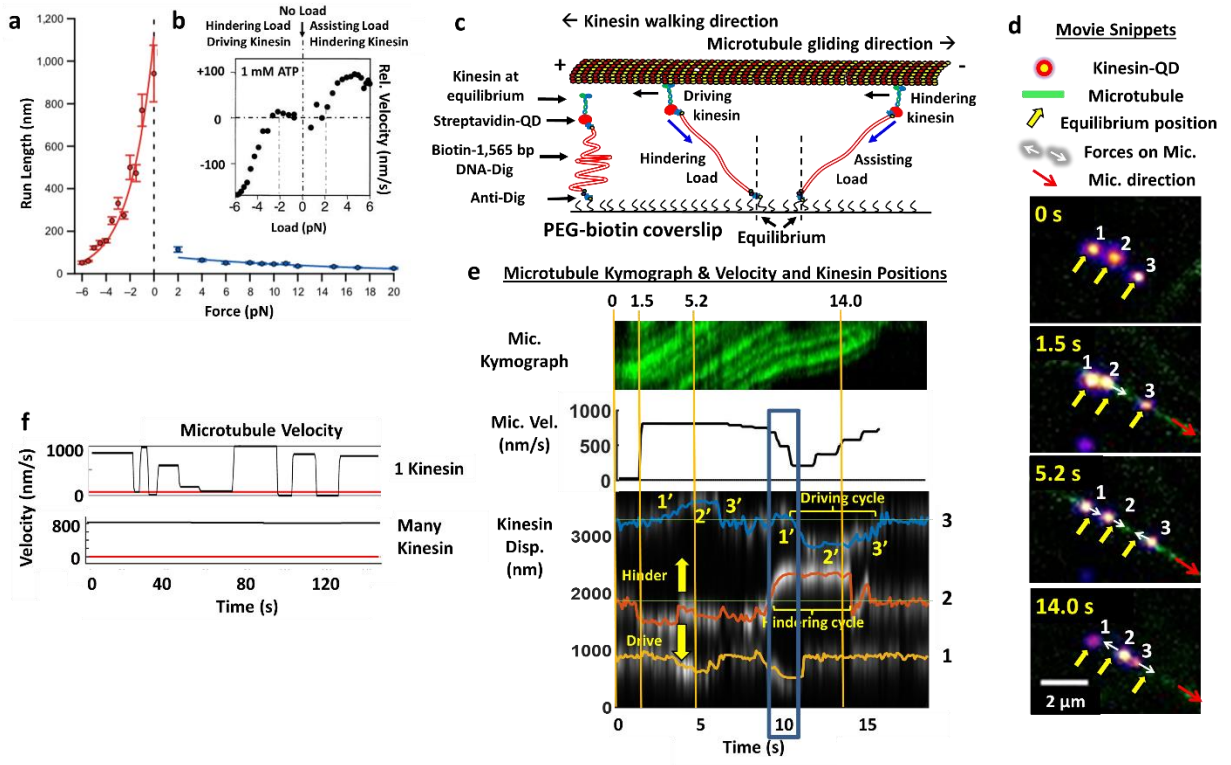

Fig. 1. Asymmetricity and force gliding assay setup. a. Kinesin run-length and velocity is asymmetric in response to load as measured in an optical trap (from[9,10]). A negative load corresponds to a force which is directed opposite to the direction that kinesin is moving the load. At negative loads the kinesin run-length drops precipitously until about -6 pN where its run-length is about the same for positive loads. **b.** The relative velocity (compared to its velocity at F=0) is very different for negative and positive forces, but is approximately equal from +/- 2 pN. **c.** Kinesin-QD is attached to 1565 base-pair DNA, which acts as a spring allowing detection of kinesin-QD movement as it drives or hinders a microtubule. Hindering kinesin moves in the same direction as microtubule while driving kinesin moves in the opposite direction with respect to their equilibrium position. Equilibrium position of kinesin is also shown. **d.** Raw images, of force-gliding assay at 0, 1.5, 5.2 and 14 sec taken every 0.2 sec (see Supplementary Movie S1). Three kinesins labeled with 705 nm QD, marked 1, 2 and 3, move a microtubule (green). Yellow arrows show equilibrium kinesin positions. White arrows point towards the direction of forces from kinesins on microtubule as kinesins are displaced from their equilibrium positions. Red arrow shows the direction of microtubule movement. **e.** Plots showing the microtubule kymograph and velocity, and kinesin positions over time (exposure time of 0.2 second). Time points 0, 1.5, 5.2, and 14 sec are marked with yellow vertical lines; from ~9-11 sec is labeled in blue for the start of the hindering cycle. Points 1', 2' and 3' are transition points for one of the hindering and driving cycle. Microtubule velocity (middle panel of 2c) starts from 0 nm/s at t = 0 sec, and increases to ~800 nm/s at frame 1.5 sec, when kinesin #2 starts driving (downward kinesin displacement). At 5.2 sec, kinesin #1 joins kinesin #2 to drive the microtubule, while kinesin #3 starts hindering. At 14 sec, kinesin #2 is hindering, kinesin #3 is driving and kinesin #1 is in equilibrium position. **f.** When a single kinesin drives the microtubule, the velocity can be very choppy as the kinesin stalls occasionally, but when several kinesins drive it, the velocity is nearly constant.

the end of the microtubule and released, resting at its equilibrium position. Kinesin #2 is hindering and kinesin #3 driving, yielding a net microtubule movement of ~500 nm/sec. From Fig. 1d,e, we can directly observe the highly dynamic and interdependent nature of multiple kinesin working together, i.e. each kinesin affects the attachment and detachment rate of another. Fig. 1f shows two additional data concerning one vs. multiple kinesins acting on a microtubule. The microtubule velocity fluctuated between 0 and ~850 nm/s when driven by a single kinesin, but remain constant

around 800 nm/s if multiple kinesins are used, one of the essential tasks fulfilled by multiple kinesins.

The fact that kinesins, while working together, attach and detach frequently, and can switch states from driving to hindering and vice versa, can be made quantitative. We averaged many such examples (17,210 time instances) similar to that shown in Fig. 1d,e. Surprisingly, we find that there is a constant percentage of kinesins which are hindering, ~35%, regardless of the total number of kinesins (from 1-8) driving the microtubule (Fig. 2a). The presence of a significant fraction of hindering kinesins appears not to have been appreciated before. Rather than one kinesin leading for a long period of time while working in a team, we find that the lead or driving kinesin is constantly changing. The average transition rate of a single kinesin is 4.9 transitions/min, of which 52% are drive-to-drive transitions (i.e. kinesin drives, then return to equilibrium, and then drives again), and ~16% are each the hinder-to-hinder, drive-to-hinder transition, and hinder-to-drive transitions (Fig. 2b). Because the transition from drive (to either drive/ hinder) position is the majority (52% + 16% = 68%), the microtubule tends to be pushed forward, despite the fact that there is considerable drag due to the presence of hindering kinesins. Fig. 2c,d shows that when kinesin is in the driving mode, it spends more time and has a longer run length on the microtubule (3.0 sec and 2.31 μm) than it does when in the hindering mode (2.15 sec and 1.43 μm). This shows that kinesin's response to force is asymmetric. We attribute this run length and duration asymmetry to kinesin's evolutionary strategy to avoid large drag force from a high fraction of hindering kinesin.

What is the size of the force that kinesin is working for, or against, under these conditions? We use a semi-quantitative method to estimate the force on the kinesin based on the extensible WLC model. Using a persistence length of 50 nm, a dsDNA contour length of 532 nm and a distance-offset of 20 nm to account for the size of QD, proteins and other attachment agents, we obtain average forces of 2.5 pN for driving and 2.1 pN for hindering kinesin (Fig. 2e). Fig. 2f shows that driving and hindering kinesin forces vary from 0-4 pN over time. The forces are on average <0.5 pN before 0.8 sec (the time for dsDNA to stretch near its contour length assuming kinesin velocity of 800 nm/s), and increases and maintained between 1-4 pN after 0.8 sec, until the kinesin detaches.

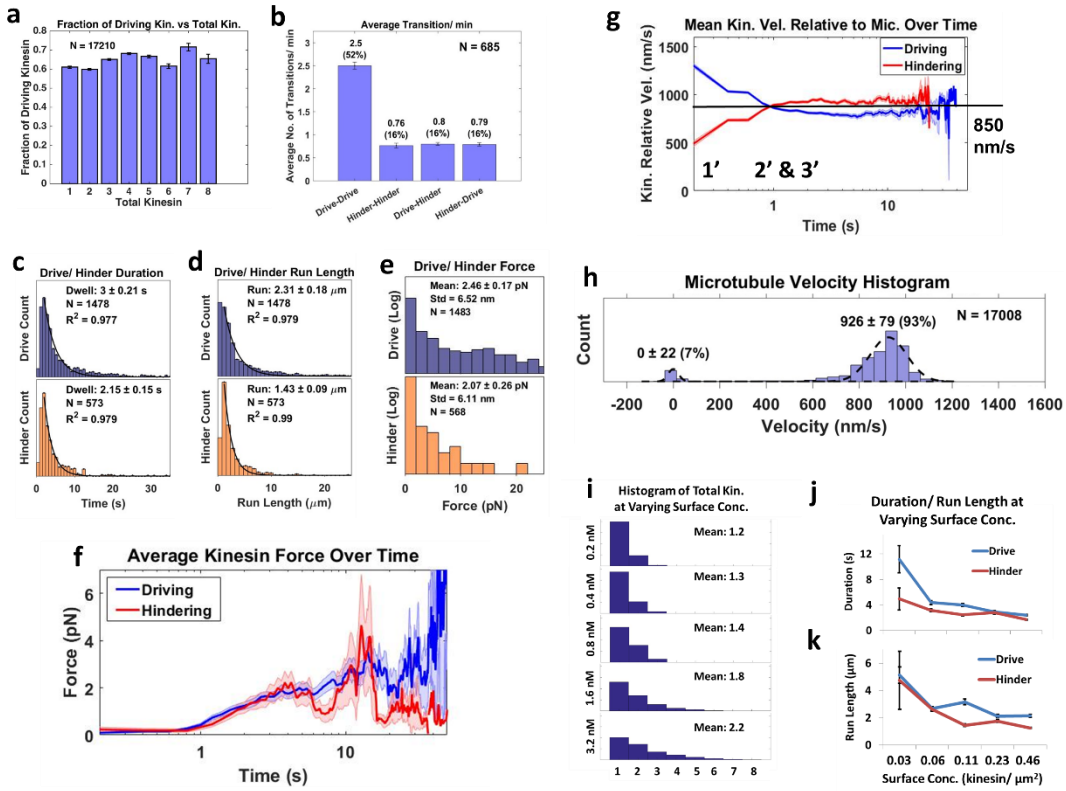

Fig. 2. Behavior of individual kinesin working in group. a. The fraction of driving kinesins remains approximately constant at around ~65% as the number of kinesin attached to a microtubule increases. **b.** The average number of transitions per minute are plotted. The major transition is from driving to driving. **c & d.** Combining all the lifetimes (durations) and run lengths from 1478 driving and 573 hindering kinesins, driving kinesin stays attached approximately 40% longer and walks approximately 62% further than the hindering kinesin, showing that hindering kinesin tends to detach more readily than the driving kinesin. **e.** An estimate for how much force the kinesin is exerting based on the eWLC. **f.** The average force exerted by driving/hindering kinesin over time increases from less than 0.5 pN for 0 to ~0.8 sec, to ~1-4 pN after 0.8 sec. Light blue and light red shadings are the standard error of the mean. **g.** The average velocity of kinesin relative to the microtubule is plotted for 960 driving kinesins and 642 hindering kinesins (detailed derivation in Supplementary Fig. S3). Driving kinesins start at a higher relative velocity (~1300 nm/s) than hindering kinesins (~500 nm/s). This is due to natural variation in kinesin velocity. Since driving and hindering kinesins are bound to the same glass slide through DNA, when they try to move the same microtubule, compressive or tensile force is built up on the microtubule as the driving kinesin tries to move microtubule faster, but the hindering kinesin moves it at a slower rate. This creates a backward force on the driving kinesin, and a forward force on the hindering kinesin, which causes the driving kinesin to slow down and the hindering kinesin to speed up. **h**, An equilibrium velocity at ~926 nm/s (plus a 7% of stationary kinesins) is reached, the average of which is approximately equal to the long term velocity of 850 nm/s shown in **g**. Regions marked 1', 2' and 3' roughly correspond to the time when kinesin started driving/hindering, reached a plateau, and returned back to equilibrium, as shown in Fig. 1e. **i.** Histogram of the total number of kinesins attached to one microtubule as kinesin surface concentration increases from 0.2 nM to 3.2 nM. As surface concentration increases, more kinesins are attached. The number of kinesins attached approximately doubles from 1.2 to 2.2 as kinesin surface concentration increases from 0.2 nM to 3.2 nM. **j & k.** The lifetime and run length of driving and hindering kinesins decreases as the kinesin surface concentration is increased from 0.2 nM to 3.2 nM, showing that as more kinesins are involved in moving the microtubule, each kinesin stays attached to and walks on the microtubule for a shorter duration and run length.

Because of the uncertainty in DNA extension (due to uncertainty in distance offset, ~0-20 nm,

and equilibrium point determination, ~0-40 nm: see Supplementary Material Section 1), significant uncertainty in force results—from sub-pN up to tens of pN—depending on the DNA extension. We thus seek to verify our force result with the published literature. In Fig. 1a, the results of Milic et al., show that run-length asymmetry is significant from −4 pN to 4 pN of force; greater than this amount, the run length becomes indistinguishable between the hindering and assisting load.[9] Since we observe run-length asymmetry, our average force range (between 0-4 pN for both driving and hindering kinesin, as in Fig. 1f) thus agree with results from Millic et al.. Fig. 1b, based on velocity, Coppin et al. give a slightly different answer. They argue that the relevant force that gives rise to asymmetric velocity response is outside the –2 pN to 2 pN range; at low load, between −2 pN to +2 pN, the velocity of kinesin is approximately constant, equal to the zero-load velocity. Because our data show that there is velocity asymmetry between -4 to 4 pN force, our result is partially in-line with the results from Coppin et al.. We should add that caution is warranted when comparing our results with those of Fig. 1a,b, since experiments in Fig. 1a,b were done with a force-feedback optical trap, and our results are for the more realistic case of a time-varying force.

We can also see the asymmetry with force between the hindering and driving kinesin by looking at the speeds when the kinesin first encounter the microtubule (Fig. 2g). On average, before interacting with the microtubule, a kinesin is at the equilibrium point; however, once bound to the microtubule, it starts to utilize ATP. The amount of ATP utilization varies randomly, leading the kinesin to be faster or slower than the microtubule, such that the DNA gets stretched towards the driving side, or hindering side, respectively (Fig. 1c). On average, the driving kinesin starts with a relative velocity (= absolute velocity of the microtubule minus absolute velocity of the kinesin) of ~1200 nm/sec and the hindering kinesin starts with a relative velocity ~500 nm/sec. However, the microtubule is going about 830 nm/sec (absolute) velocity on average (Fig. 2h, where 830 = 93%∗926 + 7%∗0). Consequently, the driving kinesin must slow down and the hindering kinesin must speed up. In both cases, DNA develops tension. For the driving kinesin, DNA pulls the kinesin backward, imposing a hindering load that causes kinesin to slow down to finally reach the steady-state (or average velocity) of microtubule movement. For the hindering kinesin, DNA pulls the kinesin forward, imposing an assisting load that causes kinesin to speed up to reach the final microtubule movement (Supplementary Fig. S1). We note that at ~1 second, the driving and hindering kinesin velocity cross. This is due to hindering and driving kinesin returning back to equilibrium, as discussed in Supplementary Material Section 2. Regions 1', 2' and 3' in Fig. 2g roughly correspond to the time when kinesin started driving/hindering, reached a plateau, and returned back to equilibrium, similar to Fig. 1e.

We next seek to find out if more kinesins can attach to the microtubule when the surface kinesin concentration increases. Past studies concluded that two kinesins transport cargo primarily via the action of one[21–23], suggesting that the number of kinesins attached to the microtubule remains the same when the kinesin concentration increases. We find the contrary. Fig. 2i shows that as the surface kinesin concentration increases from 0.03 to 0.06 kinesin/μm^2, the average number of kinesins attached to microtubule increases two-fold, from 1.1 to 2.2 kinesins. This suggests that when more kinesins are present on a cargo, more will attach, favoring plus-end transport. Note that the kinesins in our system are bound to a very large cargo (glass coverslip), and have very low stiffness when attached to long DNA, both of which increase the likelihood of many kinesins binding to a microtubule, as compared to kinesins tethered on DNA and constrained on beads used in previous published studies.

When more kinesins are involved in cargo transport, do their run length and duration remain the same? This will give insight on how well kinesins cooperate with one another. We find that the duration (Fig. 2j) and run length (Fig. 2k) of an individual kinesin decreases as more kinesins

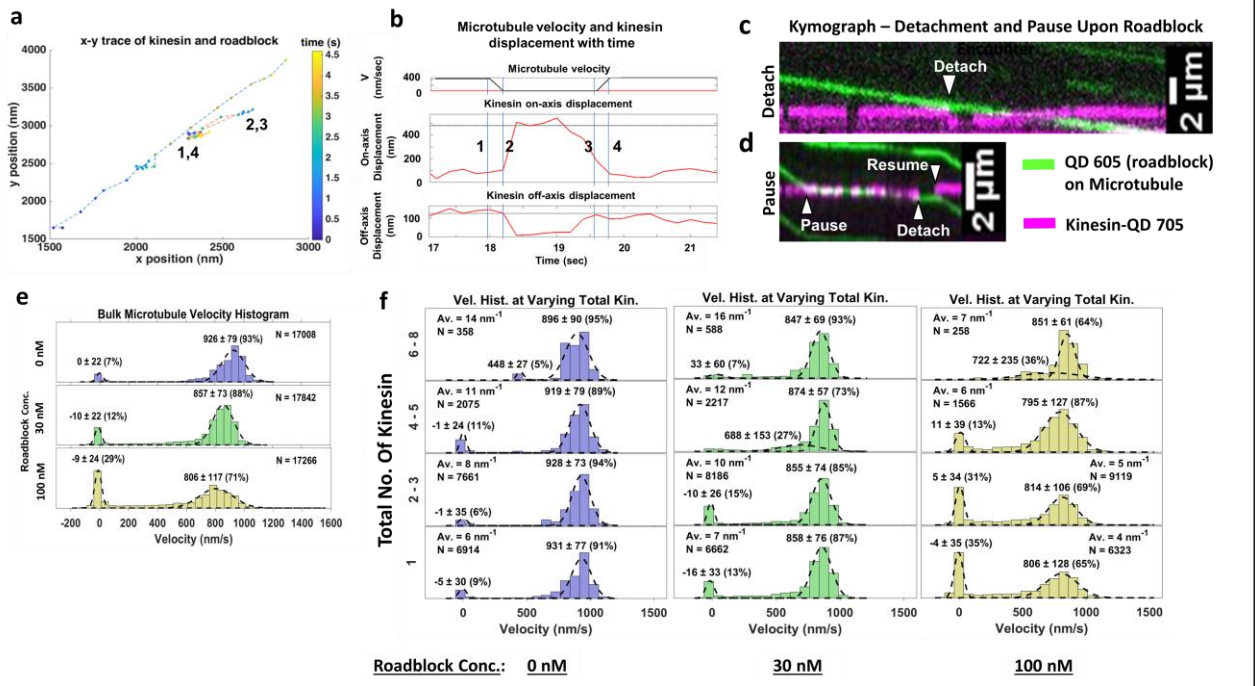

Fig. 3. Behavior of kinesin while overcoming a roadblock. a. Trajectory of a kinesin (blue) overcoming a roadblock (red) in force-gliding assay. (See Supplementary Movie S2). **b.** The kinesin and microtubule displacement and velocity. At 17 sec, the kinesin is driving microtubule at 400 nm/s until it releases at points 1 to 2 as it encounters roadblock. At points 3 and 4 the kinesin rebinds and the microtubule speeds up. Kinesin's displacement is mostly parallel to microtubule (on-axis, up to 400 nm), with just slight off-axis displacement (~100 nm). **c.** Kymograph (time at x-axis) showing detachment event (see Supplementary Movie S3) when kinesin-QD 705 (magenta) encounters roadblock (a QD 605, green) on microtubule. At the start of the kymograph, the microtubule moves downwards and kinesin-QD 705 drives the microtubule. When it hits the roadblock (at "Detach" arrow when green and magenta kymograph intersect), kinesin detaches and springs down (to its equilibrium position). **d.** Kymograph of pausing event (see Supplementary Movie S4). Kinesin-QD is initially at a slight hindering position. When it hits roadblock (at the "Pause" arrow), the microtubule stops moving until the kinesin detaches, then resumes binding microtubule and driving again. **e.** Bulk microtubule velocity histogram, showing two distinct velocity population: stuck (at 0 nm/s) and fast (at >400 nm/s). As roadblock concentration increases from 0 nM (blue) to 30 nM (green) to 100 nM (yellow), the proportion of stuck microtubule increases from 7% to 29%, while the velocity of fast microtubule decreases from 926 nm/s to 806 nm/s. **f**. With force-gliding assay, we can further classify how many kinesins move the microtubule. At higher number of kinesins, the proportion of stuck microtubule decreases, while the velocity of fast microtubule remains approximately constant.

participate in transport (i.e. when kinesin surface concentration increases from 0.03 to 0.46 kinesin/ μm^2). What is the mechanism behind this trend? Fig. 1a suggests that shorter run-length means the force on (either hindering or driving) kinesins are greater. (The effect is particularly large for hindering kinesin; less so, but still significant, for driving kinesins). Hence, our results from Fig. 2j,k suggest higher inter-kinesin tension when more kinesin participates in transport (due to higher force). What insight on kinesin's cooperativity do we gain from this trend? It is tempting—though we argue it is incorrect—to conclude that kinesins cooperate poorly with one another, since their individual duration and run length become shorter as more kinesins contribute to transport. We think this shorter duration and run length are actually beneficial, if not vital, to kinesin working as a team. Had the duration and run length increased or remain constant, the tension built up within the cargo would be so large as to cause kinesins to detach from their cargo.

How does the presence of roadblocks affect kinesin's motion? Fig. 3a, b (and Supplementary Movie S2) shows kinesin detaching from microtubule due to roadblocks. Here, an artificial roadblock is created by placing a QD (red) on the microtubule cargo. A separate QD (blue) on a single kinesin drives the microtubule at ~400 nm/s at 17.0 sec. At 18.0 sec, the kinesin encounters a roadblock, releases from the microtubule, then diffuses around on its DNA tether until it binds the microtubule again at 19.6 sec at 400 nm/sec. Fig. 3c (also Supplementary Movie S3) shows the kymograph of another kinesin detachment event. At the start of the kymograph, kinesin-QD 705 (magenta) drives the roadblock decorated microtubule, which moves downwards, shown by downward slope of the roadblock (QD 605, green) over time (x-axis). When the kinesin hits the roadblock (at "Detach" arrow), it detaches and springs down to the equilibrium before driving (moves up) the microtubule again at later time. Fig. 3d (also Supplementary Movie S4) shows kinesin pausing as it encounters roadblock. The kinesin-QD is initially at a slight hindering position. When it hits the roadblock (at the "Pause" arrow), the microtubule stops moving, shown by the horizontal green line. This pause happens for an extended period of time until the kinesin-QD detaches from microtubule (at "Detach), before reattaching again to microtubule (at "Resume") (see also Fig. S4 for another example). Overall, Fig 3a-d shows that kinesin either pauses or detaches (see Supplementary Material Section 3) when it encounters a roadblock, consistent with past studies[24,25].

How do roadblocks affect cargo (i.e. microtubule) movement? In Fig. 3e, we show the results of placing various amounts of roadblocks (0, 30 and 100 nM streptavidin-QD) onto the biotinylated microtubule. Upon plotting the velocity histograms of the microtubule, regardless of the number of kinesins (1 through ~8), we find that the histograms are well represented by two Gaussian populations: stuck (~0 nm/s) and fast (800-950 nm/s). As roadblock concentration increases from 0 to 30 to 100 nM, the proportion of stuck microtubule increases from 7% to 12% to 29%. The average velocity of the fast microtubule also decreases from 926 nm/sec to 857 nm/sec to 806 nm/sec, consistent with previous roadblock studies[26]. Taken together, roadblocks reduce the average cargo velocity and induce pauses in a cargo moved by a team of kinesin.

Because we use a gliding assay where we can determine the number of kinesins bound to the microtubule, we can further break the bulk velocity histogram down into the number of kinesin (1, 2-3, 4-5 and 6-8 kinesin), as shown in Fig. 3f. Focusing on the 100 nM roadblock result, we notice that as the number of kinesin increases from 1 to 2-3 to 4-5, the proportion of stuck microtubules decreases from 35% to 31% to 13% and eventually to zero when there are 6-8 kinesin moving the microtubule. The velocities of fast microtubules remain constant at around 805 nm/s regardless of motor number, consistent with previous studies[27]. This shows that roadblock-induced pauses can be reduced, eventually to near-zero, by having more motors available to drive the cargo. Having more motors help in two ways: 1) they continue to drive the cargo such that stuck kinesins got to hindering positions, which are more likely to be released (Fig. 2c,d); 2) their forces add up to induce higher tension on the stuck kinesin, which increases its detachment rate further (as implied by Fig. 2j,k). We postulate that multiple kinesin follow similar mechanisms in the cell to effectively transport cargo to the destination in spite of roadblocks.

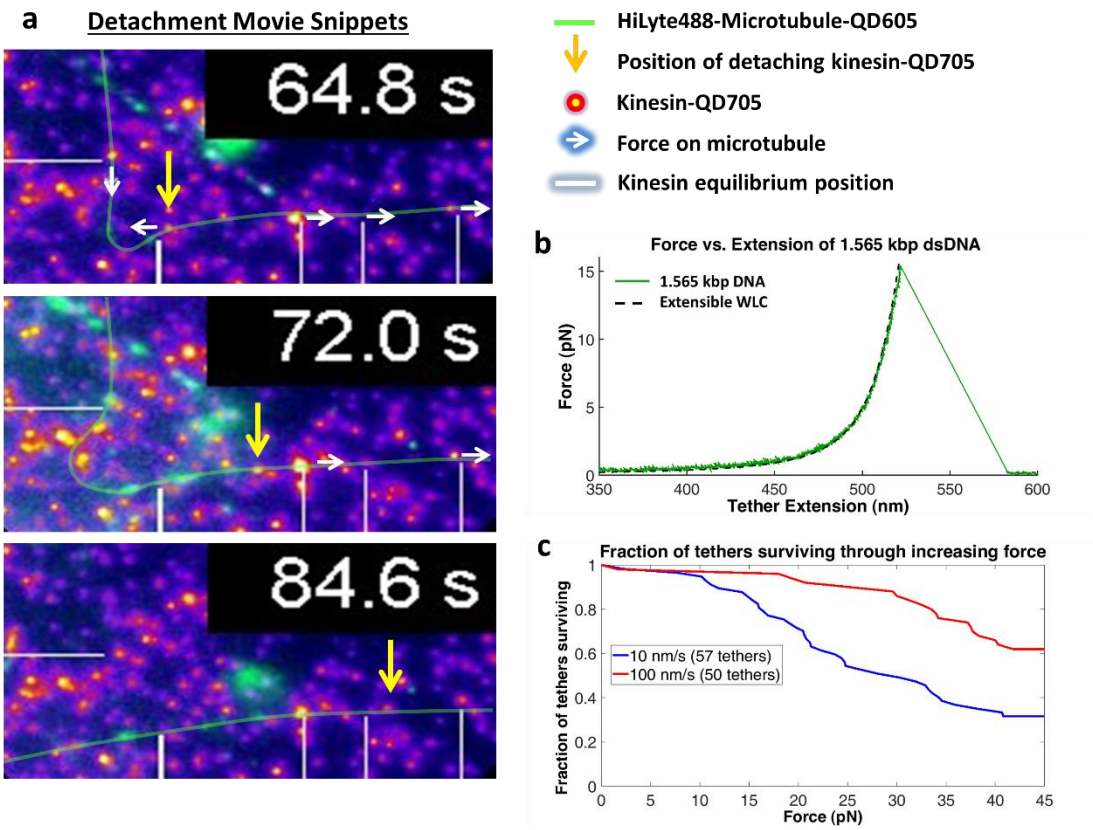

Fig. 4. Cooperative behavior of kinesin. a. Movie snippets from Supplementary Movie S5 of multiple kinesins rupturing a digoxigenin:anti-digoxigenin bond which attached one of the stuck kinesin to the coverslip. Yellow arrow shows the position the kinesin that was detached from the coverslip due to the force by multiple kinesins. **b**. Typical force extension curve of a single 1,565 kbp dsDNA obtained through a dual optical trap experiment. The digoxigenin:anti-digoxigenin rupture force in this example is ~15 pN, when DNA extension is ~520 nm. **c**. Survival probability plot for rupture force for the DNA assembly. The force indirectly represents the force production by multiple motors.

In support of the hypothesis that more motors help overcome roadblocks and reduce cargo pauses, we observed nine instances when a hindering kinesin is stuck at a roadblock while other kinesins keep driving the microtubule, causing the stuck kinesin to detach from the surface. As the hindering kinesin detaches from the coverslip, it starts moving with the microtubule, driven by a few other kinesins (Fig. 4a and Supplementary Movie S5). In Fig. 4a, at 64.8 seconds, 4 driving kinesins are pulling on a microtubule while one hindering kinesin is holding the microtubule back. The hindering kinesin is then ripped off of the glass-coverslip and the kinesin travels with the microtubule, as can be seen at 72 and the 84 sec. Presumably, the weakest link—in this case, the digoxigenin:anti-digoxigenin antibody bond for the DNA linker, is rupturing[28].

To test what the force is, and compare it to the force that a single kinesin can exert, ~6 pN, we then took the same 1.56 kb dsDNA and its linkages, and stretched it in an optical trap until the digoxigenin:anti-digoxigenin linkage ruptures (Fig. 4b; Supplementary Fig. S6; Supplementary Material Section 4). We pulled the dsDNAs at 10 nm/sec and 100 nm/sec loading rate (see Supplementary Fig. S5 for rationale) and found half of the tethers ruptured at 30 and 45 pN, respectively (Fig. 4c; Supplementary Material Section 5)[29]. These values are above the stall force of a single kinesin. Hence, the few kinesins (on average ~4) observed pulling on the detaching kinesin may exert additive forces beyond what a single kinesin can do. There is, however, an

important caveat to this argument: the unbinding may occurs at the occasional low-force end of the survival distribution, meaning it, in-fact, releases at < 6pN (see Supplementary Material Section 6).

In conclusion, our results indicate that kinesins respond to forces in an asymmetric fashion, and multiple kinesins cooperate to allow uninterrupted cargo transport, despite the presence of numerous detours and roadblocks. Fig. 5 is an example of how this might work within a cell. When one kinesin moves slower than the cargo and becomes hindering (Fig. 5a), the assisting forces from the cargo tend to increase this kinesin's speed or cause it to release rapidly, allowing the cargo to experience minimal drag force. Surprisingly, there appears to be 35% hindering kinesins, causing a continuous tug-of-war, which tends to maintain an appreciable tension between kinesins. Evolutionarily, this force asymmetry may have been tuned to increase cargo run-length (see Supplementary Material Section 7). Kinesins can rapidly switch between driving and hindering, leading to a fairly continuous and uninterrupted cargo motion forward. Against roadblocks, cooperative motion of multiple kinesins may lead to large forces, causing detachment of hindering kinesin from cargo or microtubule (Fig. 5b). Whether the tension embedded within an *in vivo* system, and whether other molecular motors such as dynein and myosin, have a similar cooperative behavior, remains to be seen.

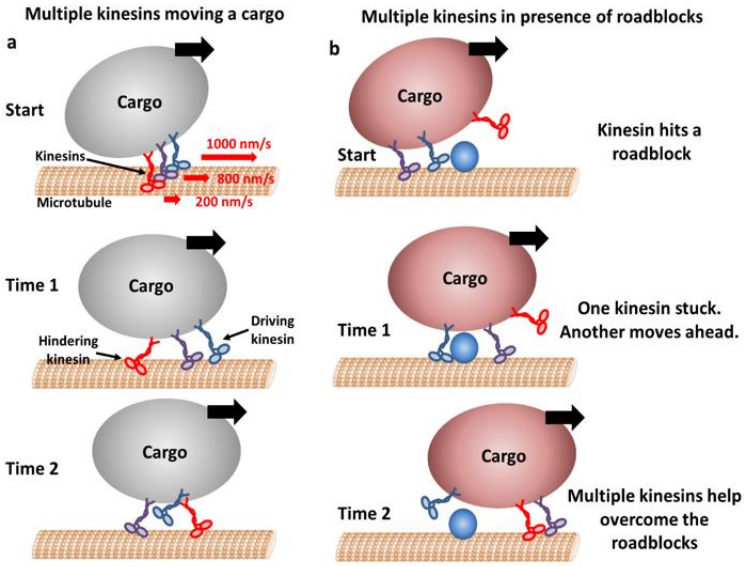

Fig. 5. Mechanism of multiple kinesin based transport. a. When working in group, different kinesins may have different velocities while starting. Red arrows represent the initial velocity values of different kinesins. Thick black arrows represent the cargo velocity direction. At “Time 1”, faster kinesins will drive, while slower kinesins will hinder the cargo. On average, one third of kinesins are hindering. Even though a hindering kinesin start slower, eventually it reaches the same velocity as driving kinesins as it feels forward tension. At “Time 2”, kinesins can detach and switch dynamically between driving and hindering. Blue kinesin has detached from its driving position and red kinesin has shifted from hindering to driving position. Hindering kinesin has shorter duration on the microtubule before detaching compared to driving kinesins. Overall, a hindering kinesin presents little resistance to the forward motion when there is no roadblock, as it detaches 33% faster than driving kinesins. **b**. In presence of roadblocks, kinesins can get stuck at the roadblock (blue kinesin at “Start” and “Time 1”). One kinesin (purple at “Time 1”) may not generate enough tension to cause detachment of hindering kinesin. However, additional kinesin(s) (red at “Time 2”) driving the cargo can generate enough force to rescue their stuck partner to resume the cargo transport.

Methods

Protein purification

Truncated kinesin with 888 amino acids (K888) from the mouse kinesin heavy chain (accession number BC090841) with a C-terminal biotin-tag and FLAG epitope, and mouse kinesin light chain (accession number BC014845) were cloned separately into the baculovirus transfer vector pAcSG2 (BD Biosciences) for recombinant virus production. Sf9 cells were infected with recombinant viruses, grown, harvested, lysed and purified using a published protocol for K888 homodimer kinesin[16]. Briefly, infected cells in growth medium supplemented with 0.2 mg/ml biotin were harvested after 72 h and lysed by sonication in lysis buffer (10 mM imidazole, pH 7.4, 0.3 M NaCl, 1 mM EGTA, 5 mM MgCl2, 7% (w/v) sucrose, 2 mM DTT, 0.5 mM 4-(2-aminoethyl) benzenesulfonyl fluoride, 5 µg/ml leupeptin) prior to clarifying at 200,000 x g for 40 minutes. The supernatant was applied to a FLAG-affinity column (Sigma-Aldrich) and washed with 10 mM imidazole, pH 7.4, 0.3 M NaCl, 1 mM EGTA. Specifically-bound protein was eluted in the same buffer containing 0.1 mg/ml FLAG peptide. Fractions of interest were combined, concentrated with an Amicon centrifugal filter device (Millipore), dialyzed against 10 mM imidazole, pH 7.4, 0.2 M NaCl, 1 mM tris(2-carboxyethyl)phosphine TCEP), 55% (v/v) glycerol,1 mM DTT, 1 µg/ml leupeptin, 50 µM MgATP, and flash frozen for storage at -80°C.

Magnetic Cytoskeleton Affinity (MiCA) purification of kinesin-QD

MiCA purification was performed to obtain one to one binding of biotinylated kinesin with streptavidin-QD 655 or 705. Briefly, kinesin K888 is mixed with 3x excess QD so that each QD has one or no kinesin bound 95% of the time. This reaction is allowed to incubate for >10 minutes on ice in a BSA-taxol buffer (1 mM THP (71194, EMD Millipore), 20 µM Paclitaxel (Cytoskeleton, Inc.) and ~30 nM ATP (Magnesium salt, A9187, Sigma Aldrich) in DmB-BSA (dynein motility buffer (30 mM HEPES, 50 mM KAcetate, 2 mM MgAcetate, 1 mM EGTA, pH 7.2) supplemented with 8 mg/mL BSA)) at 220 nM final K888 concentration and 660 nM final QD concentration. Excess QD is then removed through MiCA purification, which uses moderately positive magnetic beads (i.e. magnetic amine beads coated with PEG-amine to reduce highly positive amine charge) that bind to short microtubules to form MiCA capture beads. This is done by mixing 5 µL sonicated GMPCPP microtubule (1 mg/mL short microtubules prepared from 97% pure tubulin (HTS03-A, Cytoskeleton, Inc), stored at -80 °C and thawed right before use) with 8 µL PEG-amine magnetic beads (10 mg/mL, prepared as previously published[16]) with its buffer removed after a magnetic pull to leave only the pellet. After 5-minute incubation in an end-to-end rotator at room temperature, the MiCA capture bead is washed 2x with 8 µL BSA-taxol buffer and reconstituted in 1 µL BSA-taxol buffer to give ~1.5 µL final bead volume. Next, 6 µL kinesin-QD (220 nM kinesin) is mixed with the 1.5 µL MiCA capture bead and 1.2 µL AMP-PNP (8 mM), and the mixture is allowed to incubate for 5 minutes at room temperature in an end-to-end rotator. The AMP-PNP causes kinesin-QD to bind strongly to MiCA capture beads. The mixture is then washed 3x with 8 µL BSA-taxol buffer and 8 µL elution buffer (2 mM ATP in BSA-taxol buffer) is added. After 5-minute incubation in an end-to-end rotator at room temperature, the eluant is extracted, yielding approximately 80 nM kinesin-QD (assuming 50% purification yield).

Force-gliding assay and roadblock experiment

22 square millimeter coverslips were coated with polyethylene glycol (PEG) and biotin. Double sided tape pieces were sandwiched between a thoroughly washed glass slide and the coverslip to make the imaging channels. 600 nM streptavidin was flowed into the channel and incubated for 5 minutes. The channel was washed with DMB-BSA buffer (30 mM HEPES, 50 mM KAcetate, 2 mM MgAcetate, 1 mM EGTA, 8 mg/ml BSA, pH 7.4). 10 nM biotinylated anti-digoxigenin (Abcam) was flowed into the chamber and incubated for 5 minutes followed by a subsequent

wash with DMB-BSA buffer to remove excess anti-digoxigenin-biotin. MiCA purified kinesin-QD was mixed with 8 times less DNA (IDT) to minimize conjugation of multiple DNA molecules to single kinesin-QD. The biotin end of DNA was conjugated with the kinesin-QD and the other end with digoxigenin remained free. Kinesin-QD-DNA was flowed into the chamber and the digoxigenin end of the DNA was conjugated with the Anti-digoxigenin on the surface. The chamber was incubated with excess biotin to saturate all the streptavidin binding sites in the chamber and subsequently washed with DMB-BSA. The number of kinesins on the surface were optimized such that they were sufficiently away from each other and could be tracked individually. Finally, the imaging buffer containing the polymerized microtubules, saturating ATP and deoxygenating agents (pyranose oxidase + glucose) was flowed in the imaging chamber and movies were acquired.

For doing the roadblock experiments, biotinylated-microtubules were incubated with equal volume of streptavidin-QD605 (Thermo Fisher Scientific) solution of varying concentration (0 nM, 30 nM, 100 nM QD605). Roadblock incubated microtubules were used in the imaging buffer for doing the roadblock experiments.

Rupture force experiment with optical tweezer

Double-stranded DNA was synthesized through PCR amplification of a 1.565-kbp segment of the pBR322 plasmid (New England Biolabs), using forward and reverse primers conjugated with a 5' biotin and a 5' digoxigenin, respectively (Integrated DNA Technologies) and a high-fidelity master mix (New England Biolabs). The PCR product was purified with a PCR cleanup kit (QIAGEN).

For optical trapping experiments, 2 or 2.4 µL of 0.05 nM dsDNA were incubated for an hour at room temperature with 5 µL of 0.2% w/v streptavidin-coated beads (Spherotech). Beads were diluted in approximately 300 µL of buffer (100 mM Tris, 20 mM NaCl, 3 mM $MgCl_2$, pH 7.6) for delivery to the optical traps through bead channels in a custom flow chamber[30]. In the trapping channel of the flow chamber, dual-trap optical tweezers were used to trap a DNA-coated streptavidin bead in one trap, and a bead (Spherotech) coated with digoxigenin (Roche Diagnostics) in the other. The beads were repeatedly brought together until a DNA tether formed.

Once a dsDNA tether was formed, a force-extension curve was collected by moving one trap away from the other at a constant rate (10 nm/s or 100 nm/s) over a pre-set distance, then returning at the same rate to the initial position. Most tethers ruptured during the force ramp. Rupture is expected to occur primarily at the linkage between digoxigenin and anti-digoxinenin, as rupture forces previously reported for this linkage (under different buffer conditions) have been lower than for the biotin-streptavidin linkage[28,31]. Each resulting force-extension curve was fitted to the extensible worm-like chain model[32,33] to verify that only one molecule was present and that it behaved correctly (Fig. 4b). The maximum forces experienced by the single dsDNA tethers were determined and plotted as a survival distribution (Fig. 4c).

The optical trapping experiments were conducted in a microfluidic flow chamber[30], in a channel containing trapping buffer consisting of 76% DmB-BSA (30 mM HEPES, 5 mM $MgSO_4$, 1 mM EGTA, pH 7.0 and 8 mg/ml BSA), 10 µM biotin, 100 µM ATP, 100 µM THP, 2 µM Paclitaxel, and an oxygen scavenging system[34,35] (final concentrations in buffer: 32 mg/mL glucose, 0.58 mg/mL catalase (from *Aspergillus niger*: Millipore Sigma, formerly EMD Millipore, 219261-100KU, 5668 U/mg), 1.16 mg/mL pyranose oxidase (from *Coriolus* sp.: Sigma P4234-250UN, 12.2 U/mg), 400 µM TrisHCl and 2 mM NaCl).

Image Acquisition

Total Internal Reflection Fluorescence Microscopy (TIRFM) was performed with an inverted light microscope (Olympus IX71) equipped with two EMCCD cameras (iXon DU-897E), a TwinCam (Cairn Research) to split two colors into two separate cameras, a 100x magnification oil immersion objective (Olympus UPlanSApo, NA 1.40), and a green laser (10 mW power, Coherent OBIS 532

nm attenuated with a neutral density filter with optical density of 1.0. The excitation light was reflected with a 556 long-pass dichroic (T556lpxr-UF3 UltraFlat, Chroma) and cleaned up with 532 nm long-pass filter (BLP01-532R-25, Semrock). Fluorescence from QD and microtubule were split with a 685 nm long-pass filter (T685lpxr-UF3, UltraFlat, Chroma) in TwinCam. QD655, QD705 and a combined QD625 and HyLite 488 Microtubule emission were filtered using a 655/40 nm, 710/40, and 600/80 nm (BrightLine, Semrock) band-pass filter, respectively. Images were recorded with 0.2 seconds exposure time for all experiments, except for the experiment shown in Fig 2, where 0.1 seconds exposure time is used. An EM-gain between 10 and 300 was used, adjusted to maximize the signal collected without saturating the camera. No additional magnification was used for all experiments, except one shown in Fig. 1c-e, where 1.5x additional magnification is used. The pixel size for each image is thus 16,000 nm (the actual camera pixel dimension) / 100x objective magnification = 160 nm for most images, and 16,000 nm / 150x total magnification = 106.7 nm for those with 1.5x additional magnification.

Image Registration and Analysis

Fluorescent images obtained from the two channels of TwinCam were mapped onto each other using a transform file obtained from a set of nanohole images as previously described[16]. The 512 x 512 pixels of combined image were visualized in Fiji (plugin-rich package of ImageJ) and gliding instances of every microtubule were cropped and saved. Point locations of all kinesin-QD were detected with TrackMate[36], a plugin within Fiji, using a Laplacian of Gaussian (LoG) detector, with estimated blob diameter of 4 pixels (160 nm/pixel), threshold of 50, and sub-pixel localization turned on. Simple LAP (Linear Assignment Problem) algorithm within TrackMate was used to track all detected spots, with maximum distance for frame-to-frame linking of 4 pixels, maximum distance for track segment gap closing of 4 pixels, and maximum frame gap of 20 frames. All spots detected and tracked were then saved as a csv file for subsequent analysis in Matlab. See Supplementary Movie S6 for detailed tutorial.

In Matlab, kinesin-QD locations from TrackMate were imported, along with cropped images of microtubule and kinesin-QD. The Matlab code, FFGTraceGenerator.m, along with other necessary codes, are provided in Supplementary Material. Kinesin-QDs exhibiting driving and hindering were manually picked, and their on-axis displacements parallel to the microtubule axis were calculated after manual input of microtubule backbone. Variation in fluorescent intensity along a microtubule allows a microtubule kymograph to be generated. Edges in the kymograph were detected using the ‘edge’ command in Matlab with the ‘canny’ detection method. Manual clean-up and patching of the edges were then done to make sure microtubule movements were captured for every frame. Next, all kymograph edges were converted into velocity and averaged to obtain the microtubule velocity over time. Microtubule displacement over time was then calculated from the velocity. See Supplementary Movie S7 for detailed tutorial.

Kinesin-QD on and off-axis displacements along a microtubule were plotted and their equilibrium positions were manually identified. Drive and hinder instances were then picked with the following criteria: 1) there must be at least two points with displacements more than 100 nm or larger than 2 standard deviations from the noise at equilibrium, and 2) Traces with more than 5 seconds of missing data points are removed. All drive and hinder instances were then saved, containing information such as the duration and kinesin-QD displacement over time. Microtubule length over time was then obtained by manually identifying the microtubule backbone at select frames.

Once all the drive and hinder instances were identified for every cropped image, we compiled statistics including: the average kinesin drive-to-drive and drive-to-hinder transitions; duration, run length, and force histograms; average kinesin velocity relative to microtubule over time; bulk microtubule velocity; and microtubule velocity for specific number of kinesins attached. Force was calculated from the kinesin-QD-DNA displacement by fitting an extensible Worm-Like-Chain (WLC) model with double stranded DNA contour length of 532 nm and persistence length of 50

nm. A distance offset of 20 nm was subtracted from the kinesin-QD-DNA displacement to account for the size of QD, proteins, and PEG and to arrive at the DNA extension length.

References

1. Gross, S. P., Welte, M. A., Block, S. M. & Wieschaus, E. F. Coordination of opposite-polarity microtubule motors. *Journal of Cell Biology* **156**, 715–724 (2002).
2. McLaughlin, R. T., Diehl, M. R. & Kolomeisky, A. B. Collective dynamics of processive cytoskeletal motors. *Soft Matter* **12**, 14–21 (2015).
3. Veigel, C. & Schmidt, C. F. Moving into the cell: Single-molecule studies of molecular motors in complex environments. *Nature Reviews Molecular Cell Biology* **12**, 163–176 (2011).
4. Block, S. M., Goldstein, L. S. B. & Schnapp, B. J. Bead movement by single kinesin molecules studied with optical tweezers. *Nature* **348**, 348–352 (1990).
5. Yildiz, A., Tomishige, M., Vale, R. D. & Selvin, P. R. Kinesin Walks Hand-Over-Hand. *Science* **303**, 676–678 (2004).
6. Cai, D., Verhey, K. J. & Meyhöfer, E. Tracking Single Kinesin Molecules in the Cytoplasm of Mammalian Cells. *Biophysical Journal* **92**, 4137–4144 (2007).
7. Stamer, K., Vogel, R., Thies, E., Mandelkow, E. & Mandelkow, E.-M. Tau blocks traffic of organelles, neurofilaments, and APP vesicles in neurons and enhances oxidative stress. *J. Cell Biol.* **156**, 1051–1063 (2002).
8. Svoboda, K. & Block, S. M. Force and velocity measured for single kinesin molecules. *Cell* **77**, 773–784 (1994).
9. Milic, B., Andreasson, J. O. L., Hancock, W. O. & Block, S. M. Kinesin processivity is gated by phosphate release. *PNAS* **111**, 14136–14140 (2014).
10. Coppin, C. M., Pierce, D. W., Hsu, L. & Vale, R. D. The load dependence of kinesin's mechanical cycle. *PNAS* **94**, 8539–8544 (1997).

11. Blehm, B. H., Schroer, T. A., Trybus, K. M., Chemla, Y. R. & Selvin, P. R. In vivo optical trapping indicates kinesin's stall force is reduced by dynein during intracellular transport. *PNAS* **110**, 3381–3386 (2013).
12. Ross, J. L. The impacts of molecular motor traffic jams. *PNAS* **109**, 5911–5912 (2012).
13. Hendricks, A. G., Holzbaur, E. L. F. & Goldman, Y. E. Force measurements on cargoes in living cells reveal collective dynamics of microtubule motors. *Proc Natl Acad Sci U S A* **109**, 18447–18452 (2012).
14. Verhey, K. J., Kaul, N. & Soppina, V. Kinesin assembly and movement in cells. *Annu Rev Biophys* **40**, 267–288 (2011).
15. Kinesin Assembly and Movement in Cells | Annual Review of Biophysics. Available at: https://www.annualreviews.org/doi/full/10.1146/annurev-biophys-042910-155310?url_ver=Z39.88-2003&rfr_id=ori%3Arid%3Acrossref.org&rfr_dat=cr_pub%3Dpubmed. (Accessed: 22nd September 2018)
16. Tjioe, M. *et al.* Magnetic Cytoskeleton Affinity (MiCA) Purification of Microtubule Motors conjugated to Quantum Dots. *Bioconjugate Chemistry* **29**, 2278–2286 (2018).
17. Holzbaur, E. L. & Goldman, Y. E. Coordination of molecular motors: from in vitro assays to intracellular dynamics. *Current Opinion in Cell Biology* **22**, 4–13 (2010).
18. Hong, W., Takshak, A., Osunbayo, O., Kunwar, A. & Vershinin, M. The Effect of Temperature on Microtubule-Based Transport by Cytoplasmic Dynein and Kinesin-1 Motors. *Biophys J* **111**, 1287–1294 (2016).
19. Selvin, P. R. *et al.* Fluorescence Imaging with One-Nanometer Accuracy (FIONA). *Cold Spring Harb Protoc* **2007**, pdb.top27 (2007).
20. Bouchiat, C. *et al.* Estimating the Persistence Length of a Worm-Like Chain Molecule from Force-Extension Measurements. *Biophysical Journal* **76**, 409–413 (1999).

21. Jamison, D. K., Driver, J. W., Rogers, A. R., Constantinou, P. E. & Diehl, M. R. Two kinesins transport cargo primarily via the action of one motor: implications for intracellular transport. *Biophys. J.* **99**, 2967–2977 (2010).

22. Efremov, A. K. *et al.* Delineating cooperative responses of processive motors in living cells. *Proc Natl Acad Sci U S A* **111**, E334–E343 (2014).

23. Gutiérrez-Medina, B., Buendía Padilla, M., Gutiérrez-Esparza, A. J. & Oaxaca Camacho, A. R. Differential effect of multiple kinesin motors on run length, force and microtubule binding rate. *Biophysical Chemistry* **242**, 28–33 (2018).

24. Schneider, R., Korten, T., Walter, W. J. & Diez, S. Kinesin-1 Motors Can Circumvent Permanent Roadblocks by Side-Shifting to Neighboring Protofilaments. *Biophys J* **108**, 2249–2257 (2015).

25. Schmidt, C. *et al.* Tuning the "Roadblock" Effect in Kinesin-Based Transport. *Nano Lett.* **12**, 3466–3471 (2012).

26. Chaudhary, A. R., Berger, F., Berger, C. L. & Hendricks, A. G. Tau directs intracellular trafficking by regulating the forces exerted by kinesin and dynein teams. *Traffic* **19**, 111–121 (2018).

27. Derr, N. D. *et al.* Tug-of-War in Motor Protein Ensembles Revealed with a Programmable DNA Origami Scaffold. *Science* **338**, 662–665 (2012).

28. Neuert, G., Albrecht, C., Pamir, E. & Gaub, H. E. Dynamic force spectroscopy of the digoxigenin-antibody complex. *FEBS Letters* **580**, 505–509 (2006).

29. Moffitt, J. R., Chemla, Y. R., Izhaky, D. & Bustamante, C. Differential detection of dual traps improves the spatial resolution of optical tweezers. *Proceedings of the National Academy of Sciences of the United States of America* **103**, 9006–11 (2006).

30. Whitley, K. D., Comstock, M. J. & Chemla, Y. R. *High-Resolution Optical Tweezers Combined With Single-Molecule Confocal Microscopy*. *Methods in Enzymology* **582**, (Elsevier Inc., 2017).

31. Merkel, R., Nassoy, P., Leung, A., Ritchie, K. & Evans, E. Energy landscapes of receptor-ligand bonds explored with dynamic force spectroscopy. *Nature* **397**, 50–53 (1999).

32. Wang, M. D., Yin, H., Landick, R., Gelles, J. & Block, S. M. Stretching DNA with optical tweezers. *Biophysical Journal* **72**, 1335–1346 (1997).

33. Camunas-Soler, J., Ribezzi-Crivellari, M. & Ritort, F. Elastic Properties of Nucleic Acids by Single-Molecule Force Spectroscopy. *Annual Review of Biophysics* **45**, 65–84 (2016).

34. Landry, M. P., McCall, P. M., Qi, Z. & Chemla, Y. R. Characterization of photoactivated singlet oxygen damage in single-molecule optical trap experiments. *Biophys. J.* **97**, 2128–2136 (2009).

35. Swoboda, M. *et al.* Enzymatic Oxygen Scavenging for Photostability without pH Drop in Single-Molecule Experiments. *ACS Nano* **6**, 6364–6369 (2012).

36. Tinevez, J. Y. *et al.* TrackMate: An open and extensible platform for single-particle tracking. *Methods* **115**, 80–90 (2017).

Acknowledgements

This work was supported in part by NIH grants GM108578 and NS100019 and NSF PHY 1430124 (to PRS) and to NIH grant GM078097 (to KMT).

Supplementary Material

Supplementary Material Section 1

In our force-gliding assay, two-color Total Internal Reflection Microscopy is used to minimize background. Great care is taken to ensure that only one QD and one DNA are attached to each individual kinesin molecule, in part by employing a magnetic purification method[16] and in part by carefully optimizing the concentrations of kinesin, DNA and QDs (see Methods section). Non-specific binding of *un*labeled quantum dots and also *un*labeled kinesins on the surface are minimized through polyethylene-glycol (PEG) coating of the glass surface, and the use of bovine serum albumin (BSA) for blocking in all buffers.

Theoretically, in our assay, if we can calculate the forces exerted by all the individual kinesins driving the microtubule, we can find the total force by just summing them up. However, in our assay this is not yet feasible. First, the forces have a magnitude as well as direction and must be vectorially added. Second, there is significant uncertainty in calculating the maximal force of any given kinesin because a small uncertainty in the displacement measurement gives rise to a large uncertainty in the corresponding force calculation. Consider the force-extension curve for the 1565 bp dsDNA (Fig. 4b). The extensible worm-like chain model fits the force-extension curve very well; however, at an extension of 500 nm, for example, the slope of the DNA/WLC extension is ~1 nm/pN. Hence, a small displacement error, e.g., 10 nm would yield a possible error of 10 pN.

Supplementary Material Section 2

An interesting point in Fig. 2g is that at about 1 second, the driving and hindering kinesin velocity actually crosses as they approach the microtubule velocity (~830 nm/s). This is due to the hindering and driving kinesin returning back to equilibrium, as shown in Fig. 2c with points labeled 3'. This return to equilibrium causes hindering kinesin to increase in velocity, and driving kinesin to decrease in velocity, as shown in Supplementary Fig. S3b,d, leading to the cross-over. This cross-over takes place at an earlier time for shorter kinesin traces and a later time for longer kinesin traces.

Supplementary Material Section 3

Side-stepping, which is cited as another possibility, involves detachment then reattachment[26], and thus appears as a detachment event in our assay. We find that we are more likely to observe detachment events when we lower ATP concentration to 40 μM. At 1 mM, we mostly observe pausing events, likely because the microtubule is moving fast enough that kinesin is pushed to a hindering position and stalls microtubule progress before it detaches, or the event takes place so fast that detachment appears as a pause.

Supplementary Material Section 4

For the optical trap assay, once a tether is formed, one trap was moved away from the other at a constant rate (10 nm/s or 100 nm/s) over a pre-set distance, then allowed to return at the same rate to the initial position. For choosing the pulling rates for the optical trap experiment, we picked 9 instances of kinesin during forced detachment events. We calculated the kinesin velocity just before the forced detachment for all 9 cases (See Supplementary Fig. S5). The kinesin velocity varied between 7 nm/s to 450 nm/s, with an average of 150 nm/s. We tested 10 nm/s and 100 nm/s pulling speed in the optical trap assay to find the lowest force needed to rupture the DNA (in general, the lower the pulling velocity, the lower is the force needed to rupture the digoxigenin:anti-digoxigenin interaction). More than 50% of tethers remain at the highest force pulled (45 pN),

indicating that most of the digoxigenin:anti-digoxigenin linkage may take more than 45 pN to rupture.

Supplementary Material Section 5

Using the force to which half of the tethers survive gives a more accurate description of what the trapping experiments measure than using the average rupture force. This is because a considerable fraction of the tethers that were pulled did not rupture, but survived through a pulling and relaxing cycle. Given that the rupture value for digoxigenin:anti-digoxigenin linkage yields approximately 30 pN and 45 pN for 10 and 100 nm/s pulling rate, it is clear that the force exerted on the extracted kinesin (Fig. 4a,b) must arise from more than one kinesin pulling on it. This shows that a group of kinesins driving a cargo can exert forces much greater than a single kinesin, and thus help in smooth cargo-transport despite the presence of roadblocks.

Supplementary Material Section 6

On the survival probability plot in Fig. 4c, there is small proportion of digoxigenin:anti-digoxigenin bonds which rupture at 6 pN or less (~2-4%). We attempt to estimate the proportion of the 9 detaching kinesins over the entire population, keeping in mind that there may be more detaching kinesins which we miss. We find that there are 221 hindering kinesins that do not detach, which have similar force conditions (DNA extension > 500 nm and loading rate of <450 nm/s) as the 9 detaching kinesins. This means that the 9 detaching kinesins constitute 4% of the entire kinesin population, meaning there is a high probability that the detaching kinesins rupture at forces below 6 pN. Thus, even though we are confident that the detaching kinesin are pulled by multiple driving kinesins (on average 4), we are less certain that the forces these driving kinesins exert on the detaching kinesin are compounded beyond single kinesin stall force of 6 pN to break the digoxigenin:anti-digoxigenin bonds.

Supplementary Material Section 7

The 35% hindering kinesin (and ~65% driving kinesin) is a consequence of the asymmetric response of kinesin to force, with hindering kinesin detaching faster than driving kinesin at the same force. We propose that the strategy yielding 35% hindering kinesin is an evolutionarily optimal strategy to increase cargo run length. Without force asymmetry, hindering kinesin will detach at a rate equal to driving kinesin (a strategy yielding 50% hindering kinesin and 50% driving kinesin). In this case, faster kinesin is not favored over slower one, and the cargo run length will be less than the 35% hindering kinesin strategy. With extreme force asymmetry, hindering kinesin will detach immediately, giving 0% hindering kinesin (and 100% driving kinesin). This strategy will also yield lower cargo run length, since once the driving kinesin detaches from the microtubule, the cargo will be completely detached from microtubule.

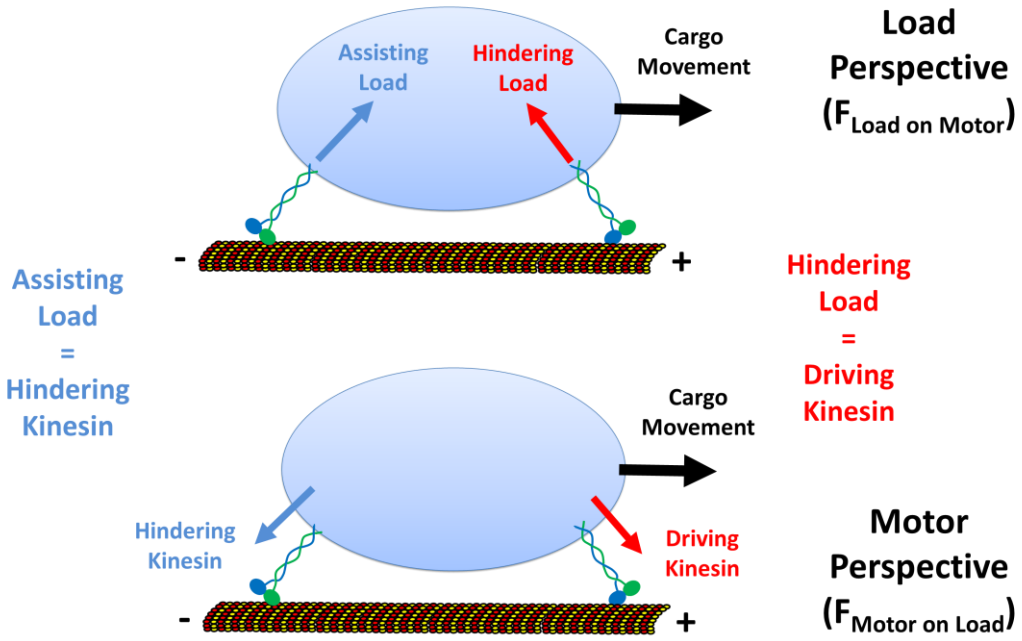

Fig. S1 | Nomenclatures for forces exerted on or by kinesin. From the load perspective, there are two types of load that can be exerted on kinesin, one is hindering load, which is in the direction opposite cargo movement, and another is assisting load, exerted in the direction of cargo movement. From the motor's perspective, a driving kinesin exerts an equal but opposite force as the hindering load. Likewise, a hindering kinesin exerts an equal but opposite force as the assisting load.

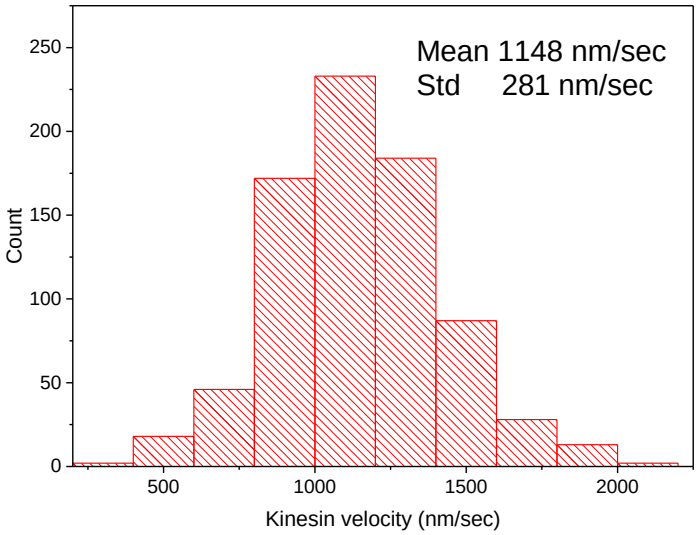

Fig. S2 | Walking velocity of single kinesin: Single kinesins were labeled with QD705 and their motion was observed in immobilized microtubules under saturating ATP concentration. Kinesin moved with a speed of 1148 ± 281 nm/sec.

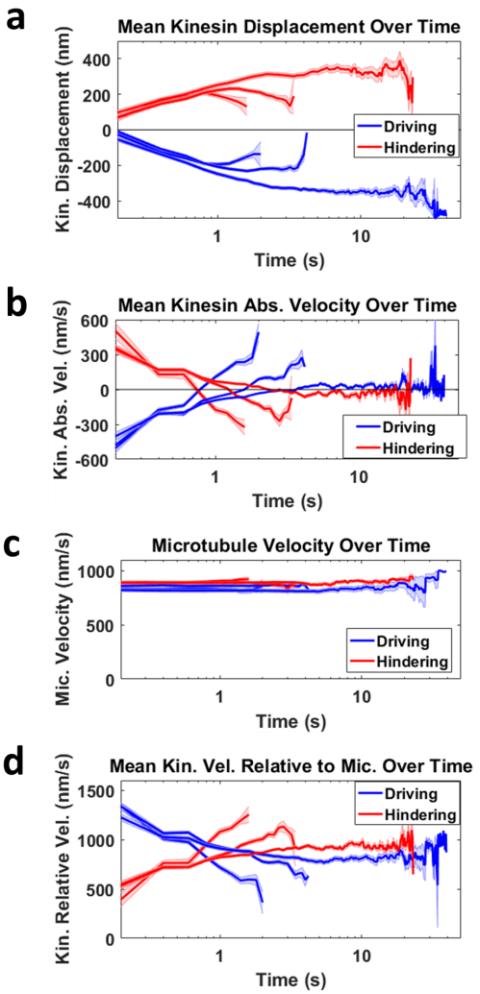

Fig. S3 | Deriving mean kinesin velocity relative to microtubule. a. The mean kinesin displacement over time is shown for three groups of kinesin sorted based on the duration of it driving (blue) or hindering (red). The shortest group has a duration up to ~2 s, followed by the second longest group with duration up to ~4 s, and the longest group stays attached to microtubule up to ~40 s. Light blue and red shading for all graphs refer to the standard error of the mean. **b.** The mean kinesin absolute velocity over time is the first derivative of the mean kinesin displacement over time shown in **a**. Notice that all the graphs in **b** cross the zero velocity line at the turning point of the graphs in **a**. **c.** Mean microtubule velocity over time for all the three driving and hindering groups. The microtubule velocities range between 800 – 900 nm/s and the mean of the groups are approximately constant over time. **d.** The mean kinesin velocity relative to microtubule over time is calculated by subtracting the microtubule velocity over time (**c**) with the mean kinesin velocity over time (**b**).

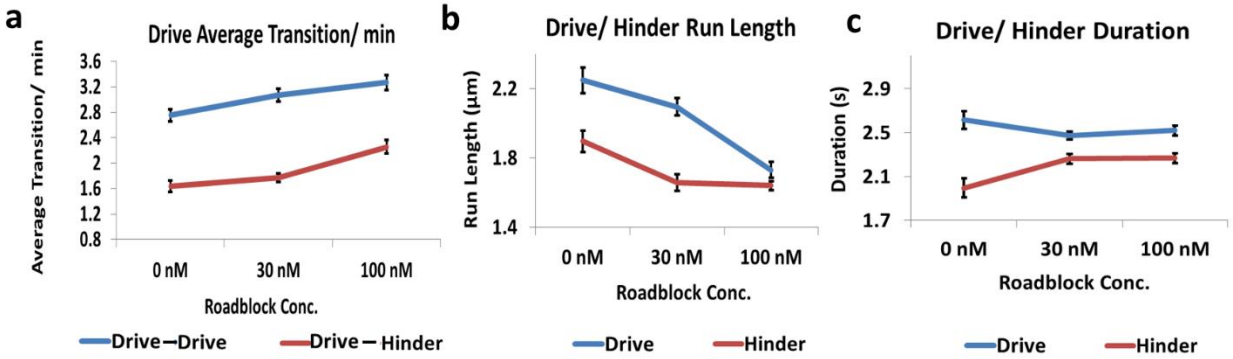

Fig. S4 | Kinesin either pauses or immediately detaches upon encountering roadblocks. A roadblock disrupts driving instances, causing driving kinesin to transition to hindering (drive-to-hinder) when pausing, or back to equilibrium before attempting another instance of driving (drive-to-drive) or hindering (drive-to-hinder) when detaching from the microtubule. **a**. Detachment and pausing events result in the increase in drive-to-drive and drive-to-hinder transitions as roadblock concentration increases from 0 to 100 nM. **b.** Kinesin run length decreases for both driving and hindering kinesins when the roadblock concentration increases. This is because detachment and pausing instances due to roadblock terminate driving and hindering runs. **c.** The trend for driving/hindering duration differs from that for run length. Driving duration decreases from 0 to 100 nM while hindering duration increases from 0 to 100 nM. This is because pausing instances affect driving and hindering duration differently. Pausing decreases driving duration, since driving kinesin will transition into hindering during a pausing event, prematurely ending the driving run and thus duration. Hindering kinesin, on the other hand, will stay bound to microtubule during a pausing event and remain registered as hindering, increasing the hindering duration.

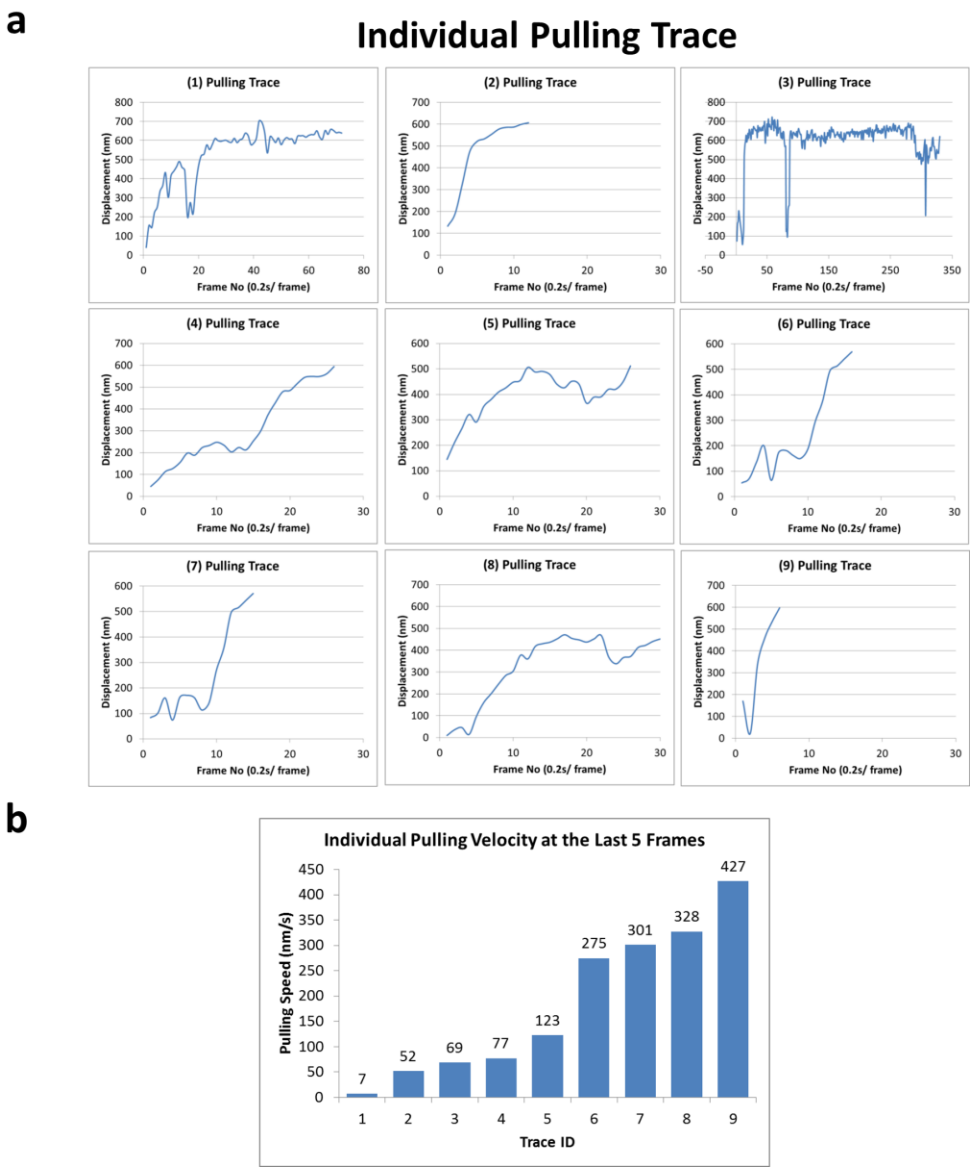

Fig. S5 | Forced detachment traces and velocities. a. Nine pulling traces right before forced detachment of kinesin-QD, rupturing supposedly the weakest link in the coverslip-DNA-QD-kinesin interaction, which is the digoxigenin:anti-digoxigenin interaction. **b.** The velocities of the last five frames before the forced detachment for all nine traces. The velocities (of kinesin relative to the glass coverslip) vary from 7 nm/s to 427 nm/s.

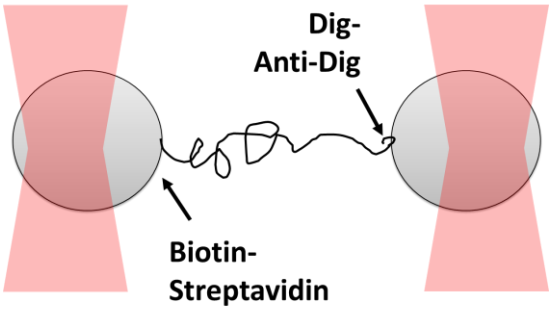

Fig. S6 | Dual optical trap assay to measure the rupture force for digoxigenin:anti-digoxigenin interaction. Two polystyrene beads are bound to the opposite ends of 1,565 bp DNA through biotin-streptavidin linkage and digoxigenin:anti-digoxigenin linkage, which is the weaker of the two. The beads are captured in optical traps and are pulled away from one another until the digoxigenin:anti-digoxigenin linkage ruptures.